

Article

Adhesion Forces of Shale Oil Droplet on Mica Surface with Different Roughness: An Experimental Investigation Using Atomic Force Microscopy

Ting'an Bai¹, Feng Yang^{1,2,*} , Huan Wang¹ and He Zheng¹

¹ Key Laboratory of Theory and Technology of Petroleum Exploration and Development in Hubei Province, China University of Geosciences, Wuhan 430074, China

² Key Laboratory of Petroleum Resources Research, Lanzhou 730000, Gansu Province, China

* Correspondence: fengyang@cug.edu.cn

Abstract: In order to investigate the effect of rock surface roughness on the occurrence state of shale oil, muscovite mica was firstly characterized by performing atomic force microscopy (AFM). Two-dimensional (2D) images and the three-dimensional (3D) structure of the mica surface were obtained. Wettability of the micas was measured according to the sessile drop method using shale oil, collected from a lacustrine shale oil well drilling through the Yanchang Formation, Ordos Basin. Then, the adhesion forces between shale oil and mica surface with a different roughness were finely measured using AFM mounted with the shale oil modified probe tips. The adhesion force curves at the approaching and retract modes were obtained. The results show that the average roughness value of the mica samples was about 1 nm, while the maximum height was up to 4 nm. The contact angle between shale oil and mica ranged from 128.73° to 145.81°, and increased with increasing surface roughness, which can be described by the Wenzel model. The adhesion force between shale oil and mica also increased with an increasing contact area. Shale oil can fill the deep valleys on the rough surface of rocks and then form microscopic storage for oil droplets. The maximum adhesion force, reached at a distance of about 5–10 nm between shale oil droplets and micas, was between 14 and 30 nN. The adhesion force disappeared when the distance was larger than 40 nm. These indicate that shale oil in pores with a diameter of less than 10 nm was tightly adsorbed, and formed a layered accumulation pattern. Additional energy is needed to decrease the disjoining pressure and then separate shale oil from these tight pores. Shale oil is freely movable at pores with pore diameters of larger than 40 nm. This work provides a new insight about the interaction between shale oil and rock, and helps to understand the occurrence mechanism of shale oil.

Keywords: shale oil; adhesion force; contact angle; AFM; roughness; occurrence mechanism



Citation: Bai, T.; Yang, F.; Wang, H.; Zheng, H. Adhesion Forces of Shale Oil Droplet on Mica Surface with Different Roughness: An Experimental Investigation Using Atomic Force Microscopy. *Energies* **2022**, *15*, 6460. <https://doi.org/10.3390/en15176460>

Academic Editors: Reza Rezaee and Dameng Liu

Received: 28 July 2022

Accepted: 1 September 2022

Published: 4 September 2022

Publisher's Note: MDPI stays neutral with regard to jurisdictional claims in published maps and institutional affiliations.



Copyright: © 2022 by the authors. Licensee MDPI, Basel, Switzerland. This article is an open access article distributed under the terms and conditions of the Creative Commons Attribution (CC BY) license (<https://creativecommons.org/licenses/by/4.0/>).

1. Introduction

Oil–rock interaction plays an important role in petroleum science and engineering. The adhesion force between oil and rocks controls the occurrence state and flow capacity of oil in pore systems of underground reservoirs. In recent decades, the enhanced oil recovery of tight reservoirs by the injection of carbon dioxide, light hydrocarbons, and low salinity water has been widely used in laboratory and field operations [1,2]. Many of these techniques aim to improve the flow capacity of crude oil by reducing its viscosity [2]. However, the flow capacity of crude oil through pores is not only affected by viscosity, but also rock surface properties such as wettability, interfacial tension and adhesion force. It is challenging to understand the interaction mechanism between crude oil and rocks because of its complexity.

Wettability, a key parameter controlling the oil occurrence state and movability, is related to interfacial energy. The contact angle is usually used to characterize the wettability of rocks. When the gas–liquid–solid or liquid–liquid–solid is at an equilibrium state, the

relationship between the contact angle and three-phase interfacial tension can be quantitatively described according to Young's equation [3]. However, fine-grained sedimentary rocks, such as shales, appear to be complex in terms of wettability due to the varied mineral compositions and additional hydrocarbon adsorption. Some scholars believed shales to be water-wet, while others reported an oil-wet property, and even a mixed wettability of shales [4,5]. As for shale oil movability, investigators used a pore network to simulate the fluid flow in shale formations, and thought that different kinds of pores in shales affect the oil flow capacity [6–9]. Despite the fact that this subject has been explored widely in recent years, the internal reasons for these variations still remain unclear. In addition, the surface roughness of rocks also affects the contact angle and wettability [6].

Adhesion force in the oil–rock interaction controls the surface behavior of rocks. The adhesion force is a microscopic force, and can be measured using atomic force spectroscopy (AFM), surface forces apparatus (SFA), or quartz crystal microbalance (QCM) [10–13]. Recently, Zhu et al. [14] investigated the wettability and adhesion of water on coals using QCM during coal flotation, and found that the contact angle decreased with an increasing roughness of coals. The adhesion force between water droplets and coal with a rough surface is large, which is due to the increase in the contacted surface area and the appearance of a ridge line of rough surface [14]. Some researchers used the QCM to investigate the adsorption and desorption of crude oil on quartz surfaces at flowing conditions and estimated the thickness of adsorbed oil [10]. SFA was applied to compare the interaction behavior of diluted bitumen (DB) and conventional crude oil (CCO) with a smooth mica surface in toluene solution [11]. It was observed that CCO exhibits an adsorption behavior which is different from DB at the tested concentrations. This different adsorption behavior is mainly caused by the high concentration of surfactants such as asphaltenes. Other researchers also used SFA to study the adsorption of asphaltenes on mineral surfaces, and found that asphaltenes from organic solvents adsorb minerals and their interactions were affected by mineral type, adsorption time and asphaltene concentration [15]. In recent years, AFM was introduced to the petroleum industry and used in the characterization of surface properties of minerals due to its high sensitivity and comprehensive functions [16–18]. The PeakForce-Quantitative Nanomechanical Mapping (PF-QNM) mode in atomic force microscopy is used to quantitatively characterize the mechanical properties of various mineral components in organic-rich shales, including Young's modulus and Poisson's ratio [19]. The elastic modulus of organic matter in shale is significantly different from inorganic minerals and is related to thermal maturity [19]. In addition, with the addition of a modified probe, atomic force microscopy can be used to measure the interaction behavior between liquid and solid. An oil coated probe after crude oil modification was developed to directly measure the crude oil and mineral interactions at natural length scales in different solution environments [20]. The results show that the repulsive force decreases with an increase in the monovalent ion concentration, which is consistent with the Debye–Hückel theory. Some researchers modified the probe by applying chemical bonding, a method called chemical force microscopy (CFM) [21,22]. CFM is a newly used technique in the assessments of wettability and oil–mineral adhesion forces by utilizing hydrophobic (CH₃-terminated) functionalized probes. However, this method used methyl groups to simulate crude oil droplets, which is not completely consistent with the crude oil in reservoirs. In addition, this method is difficult to perform [23–25].

In this work, the adhesion behaviors of shale oil on muscovite mica surfaces were systematically studied by performing multiple techniques. The surface roughness of mica was characterized using two-dimensional (2D) and three-dimensional (3D) images scanned by AFM. The wettability of the micas was also measured following the sessile drop method. Then, the adhesion forces between the shale oil and mica surface with a different roughness were measured using the PF-QNM mode of AFM. The effect of roughness on the adhesion force between the mineral surface and oil droplets was discussed. This microscopic analysis of oil–rock interaction improves the understanding of hydrocarbon occurrence and flow in

tight shales. As far as we know, this is the first time that the adhesion between shale oil and rocks at a very fine level is reported.

2. Materials and Methods

2.1. Materials and Tips Functionalization

2.1.1. Crude Oil of Shales

Crude oil was collected from a shale oil well drilling through the Yanchang Formation in the Ordos Basin, China. To avoid exposure to light and contamination, the crude oil sample was collected and quickly sealed in brown reagent bottles. Then, the chemical compositions of the crude oil were tested and presented in a mass fraction (Figure 1). C_1 – C_5 hydrocarbons accounted for 1.16% of all hydrocarbons, C_6 – C_{14} hydrocarbons accounted for 23.32% of all hydrocarbons, and C_{15+} hydrocarbons were the largest component, accounting for more than 75% of all hydrocarbons.

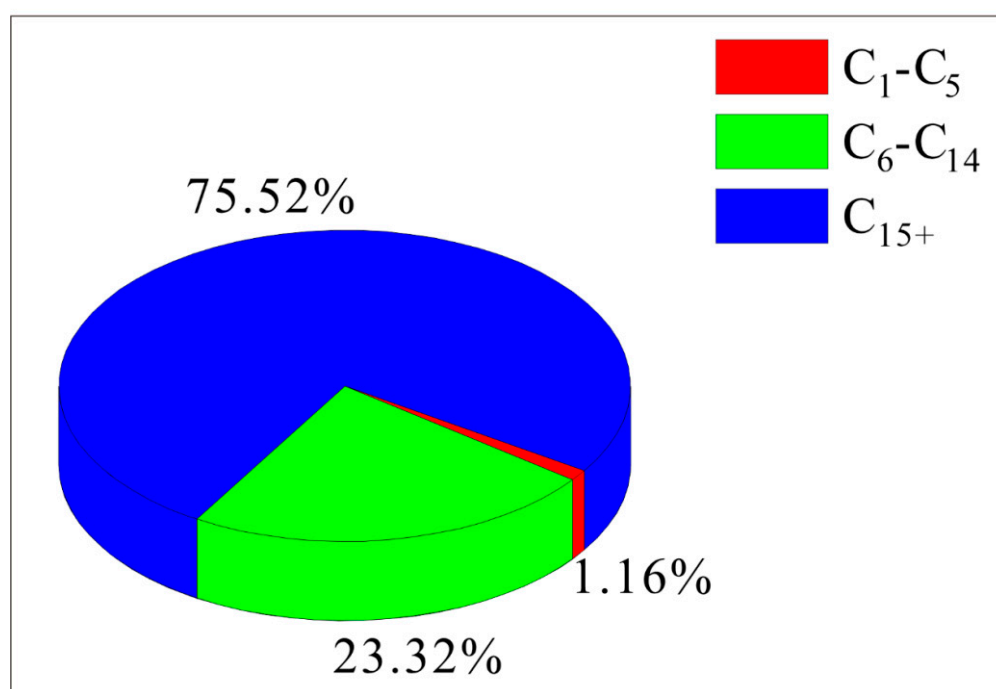


Figure 1. The chemical composition of crude oil collected from a shale oil well drilling through the Yanchang Formation, Ordos Basin.

2.1.2. Base Material

Natural mica has an obvious lamellar structure, high level of hardness, hard deformation and stable chemical properties. In atomic force microscopy (AFM) scanning experiments, excessive fluctuations in rock surface easily damage the probe tip and cause artifacts, which leads to the inaccurate representation of the true surface property of the sample. High quality mica can achieve a moderate smooth surface, which is an ideal base material for atomic force microscopy scanning and force curve measurements. The muscovite mica in this study was purchased from S&J Trading Inc. (New York, NY, USA). A layer of mica was carefully peeled off using a tape before the experiments.

2.1.3. Tips Functionalization

There are several kinds of probe tips that can be used for atomic force microscopy scanning [26,27]. The spherical probe tips are not sensitive to changes in the surface morphology and may cause artifacts during testing. Additionally, spherical probe tips easily form liquid bridge behavior with the droplet surface, resulting in artificial errors in force curve measurements. To avoid these defects, sprayed tips (SNL-10, Bruker) were used

in this study. The probe tips were modified before experiments. Firstly, a drop of crude oil was placed on the surface of the mica. Then, the cantilever beam of AFM was moved so that it was above the oil droplet, and then the probe tip was slowly lowered to approach the crude oil droplet. After the probe tip contacted the oil droplet for 2 s, the probe tip was lifted up to a safe position. This process can be checked in the eyepiece of the atomic force microscope. The mica surface changes slightly after modification, and then it is accepted that the oil droplets are modified on the surface of the probe tip.

2.2. Roughness Measurements

Atomic force microscopy was used to scan the mica surfaces. Then, the NanoScope analysis software was used for the AFM images to quantitatively characterize surface roughness. The roughness can be expressed by two parameters, including the average roughness (R_a) and the root mean square roughness (R_q). The average roughness R_a reflects the average distance of the sample surface deviated from the datum plane, while the root mean square roughness R_q reflects the root mean square distance of the sample surface deviated from the datum plane. Their calculation formulas are expressed as follows:

$$R_a = \frac{1}{N_x N_y} \sum_{i=1}^{N_x} \sum_{j=1}^{N_y} |Z(i, j) - Z_{mean}| \quad (1)$$

$$R_q = \sqrt{\frac{1}{N_x N_y} \sum_{i=1}^{N_x} \sum_{j=1}^{N_y} (Z(i, j) - Z_{mean})^2} \quad (2)$$

where N_x and N_y are the number of scanning points along the X-axis and Y-axis of the image, respectively; $Z(i, j)$ is the height value of the point where the coordinates (i, j) are located in the image; and Z_{mean} is the average height of all scanning points in the AFM image.

The AFM instrument used in this experiment is the Dimension Icon AFM manufactured by the Bruker Company, Germany. The maximum scanning range was $90 \mu\text{m} \times 90 \mu\text{m} \times 10 \mu\text{m}$, and the resolution was 0.15 nm in the lateral direction and 0.04 nm in the vertical direction.

2.3. Contact Angle Measurements

The contact angle was measured using JC2000DM (China) according to the sessile drop method. During the experiments, a volume of about $8 \mu\text{L}$ of shale oil was dropped slowly from the capillary port to the surface of the mica. A high-frequency camera was constantly taking pictures of the crude oil drops until they were completely stable. After that, the ImageJ2022 (NIH, USA) software was used to treat the photos to obtain the contact angles.

2.4. Adhesion Force Measurements

AFM was utilized to quantitatively characterize the adhesion force between shale oil and rocks with different roughness. The probe tip of the AFM was placed close to the sample surface and the deflection (D) of the cantilever beam was detected by the laser beam. The measured deflection was taken into Hooke's law ($F = k \times D$) to calculate the force (F). The actual spring constant of the cantilever beam was determined by the thermal tuning method, proposed by Hutter and Bechhoefer [28]. The probe deflection sensitivity was recalibrated before every experiment.

The interaction between the fluid in the probe tips and the solid surface can be described by the classical Derjaguin–Landau–Verwey–Overbeek (DLVO) theory [27], which mainly considers the van der Waals forces (F_{vdw}) and electrical double layer forces (F_{edl}).

$$F_{edl} = 4\pi\epsilon_0\epsilon\psi_1\psi_2(a_0e^{-\kappa D} - a_1e^{-\kappa L_1}) - 2\pi\epsilon_0\epsilon(\psi_1^2 + \psi_2^2)(a_2e^{-2\kappa D} - a_3e^{-2\kappa L_1}) + \frac{4\pi\epsilon_0\epsilon\kappa}{\tan\alpha} \left[b_1\psi_1\psi_2e^{-\kappa L_1} + b_1\frac{\psi_1^2 + \psi_2^2}{2}e^{-2\kappa L_1} \right] \quad (3)$$

$$F_{vdW} = \frac{A_{123}}{6} \left[\frac{R + D - 2L_1}{L_1^2} - \frac{R - D}{D^2} \right] - \frac{A}{3 \tan^2 \alpha} \left(\frac{1}{L_1} + \frac{R \sin \alpha \tan \alpha - D - R(1 - \cos \alpha)}{2L_1^2} \right) \quad (4)$$

where ψ is the surface potential; ε the relative permittivity of medium; ε_0 the permittivity of vacuum; κ^{-1} is the Debye length; R is the tip radius; α is the geometric angle for the spherical cap at the tip end; D is the separation distance between the tip and the sample surface; A_{132} is the Hamaker constant for the tip and the sample surface interacting across water; and Subscripts 1 and 2 refer to the tip and the sample surface, respectively. Other parameters are given by:

$$L_1 = D + R(1 - \cos \alpha) \quad (5)$$

$$a_0 = \kappa R - 1 \quad (6)$$

$$a_2 = a_0 + 0.5 \quad (7)$$

$$a_3 = a_1 + 0.5 \quad (8)$$

$$b_1 = \left[R \sin \alpha - \frac{D + R(1 - \cos \alpha)}{\tan \alpha} \right] + \frac{1}{\tan \alpha} \left(L_1 + \frac{1}{\kappa} \right) \quad (9)$$

$$b_2 = \left[R \sin \alpha - \frac{D + R(1 - \cos \alpha)}{\tan \alpha} \right] + \frac{1}{\tan \alpha} \left(L_1 + \frac{1}{2\kappa} \right) \quad (10)$$

3. Results

3.1. Surface Roughness

The surface of micas was scanned using an atomic force microscope and then the digital images were treated using NanoScope Analysis software. Figure 2 shows the surface morphology of three mica samples in three dimensions. There are many valleys and peaks in the sample surface in the 3D surface structure. Compared to the datum plane, the maximum and minimum height values of the sample surfaces were -2.4 – 2.2 nm. That means that the drop height of the sample surfaces was up to 4.6 nm. In order to clearly show the surface fluctuation of the mica samples, the 2D plan sections of the mica samples are shown in Figure 3a, and the surface height of the section, both parallel and perpendicular to texture, are shown in Figure 3b. The height difference parallel to the texture direction (red line) is about 1 nm, while the height difference perpendicular to texture direction (blue line) is about 3 nm. This means that the mica surface is not absolutely smooth.

According to the height values, the roughness values of samples (average roughness R_a and root mean square roughness R_q) were calculated and summarized in Table 1. The R_a and R_q values of Sample A are 0.51 nm and 0.648 nm, respectively. The R_a and R_q of Sample B are 0.402 nm and 0.505 nm, respectively. The R_a value of the Sample C is 0.363 nm and the R_q value is 0.463 nm. Among these three mica samples, the surface of sample C was the smoothest. For a given sample, the R_a value is less than the R_q value. The R_q values are much more sensitive to the morphology variation of the surface. Small fluctuations in surface height lead to great variations in the root mean square roughness.

Table 1. Sample average roughness, root mean square roughness and contact angle of mica samples.

Mica Sample	Average Roughness (R_a , nm)	Root Mean Square Roughness (R_q , nm)	Contact Angle ($^\circ$)
A	0.510	0.648	145.81 \pm 3.0
B	0.402	0.505	135.52 \pm 4.5
C	0.363	0.463	128.73 \pm 2.0

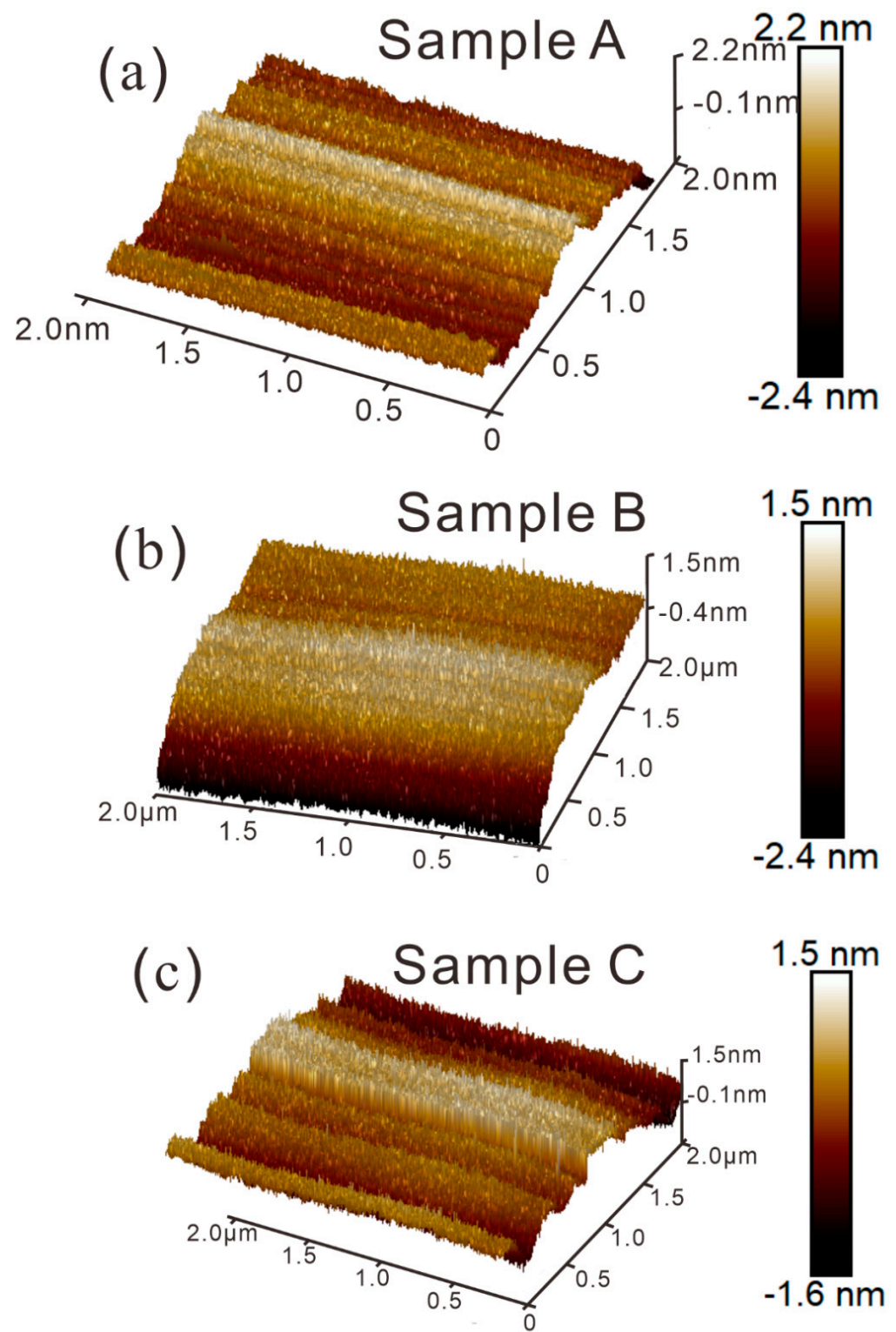


Figure 2. 3D surface structure of the mica samples scanning by AFM: (a) Sample A; (b) Sample B; (c) Sample C.

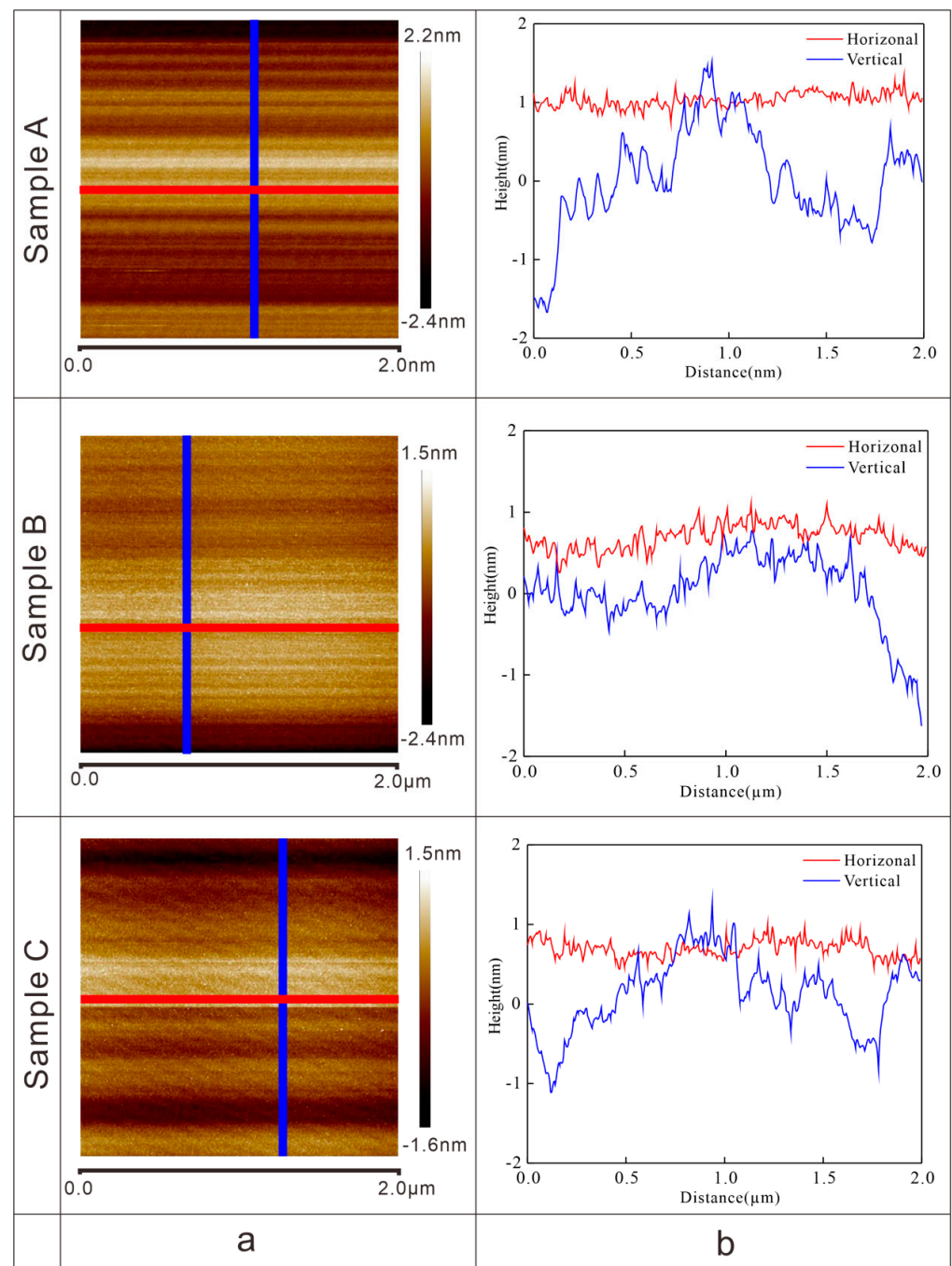


Figure 3. (a) 2D plan sections of the mica samples; (b) the surface height of the section parallel and perpendicular to texture.

3.2. Wettability

The contact angle of shale oil on mica surfaces ranged from $128.73^\circ (\pm 2.0^\circ)$ to $145.81^\circ (\pm 3.0^\circ)$, which was measured using the sessile drop method. Surface roughness and morphology fluctuation affect the wettability of rock. Figure 4 shows the relationship between the roughness of the mica samples and measured contact angle. Mica sample A has a contact angle of $145.81^\circ (\pm 3.0^\circ)$ for shale oil while its average surface roughness is 0.51 nm. Mica sample B has a contact angle of $135.52^\circ (\pm 4.5^\circ)$ and average surface roughness of 0.402 nm. The smoothest mica sample C has the smallest contact angle of $128.73^\circ (\pm 2.0^\circ)$, and the lowest average roughness of 0.363 nm. These results indicate that the contact angle increases with increasing surface roughness.

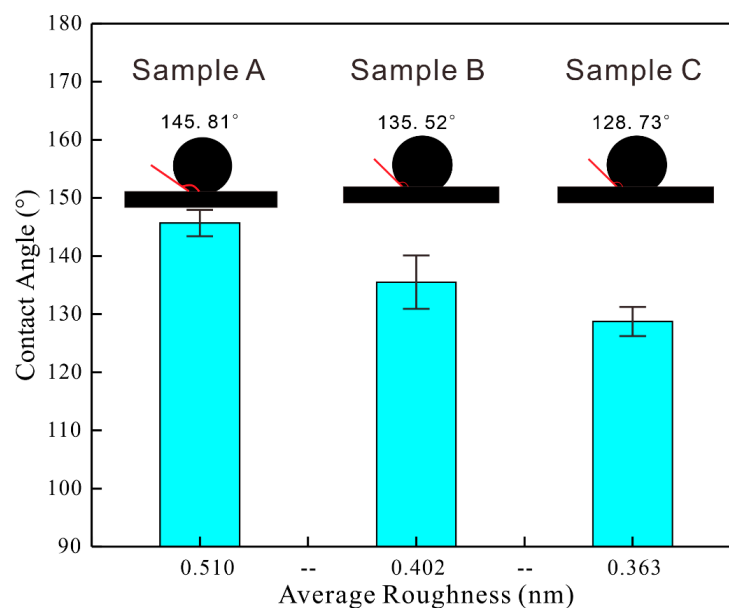


Figure 4. The relationship between roughness and contact angle of mica samples.

3.3. Adhesion Force between Crude Oil and Mica

In order to study the interaction between the oil and mica surface, the adhesion force was measured using AFM, and the effect of roughness on the occurrence of oil was further analyzed. Using the oil-coated probes, force spectroscopy measurements were carried out on mica substrates. Figure 5 shows the adhesion force curves of the oil-coated probe on mica samples. The black curve is the force curve when the probe tip approaches the sample, while the red curve is the force curve when the probe tip is retracted. It can be observed that the repulsive force gradually increases when the probe tips approach the sample surface, which indicates the existence of repulsion between shale oil droplets and the mica surface. The repulsion generally occurs at a distance of about 5 nm. When the probe tip begins to move away from the surface of the mica, the repulsive force gradually decreases while the attraction force begins to increase. The maximum attraction force is reached at a distance of about 5–10 nm. Then, the attraction force decreases very quickly when the distance increases to 15 nm, and gradually vanishes after the distance being greater than 40 nm.

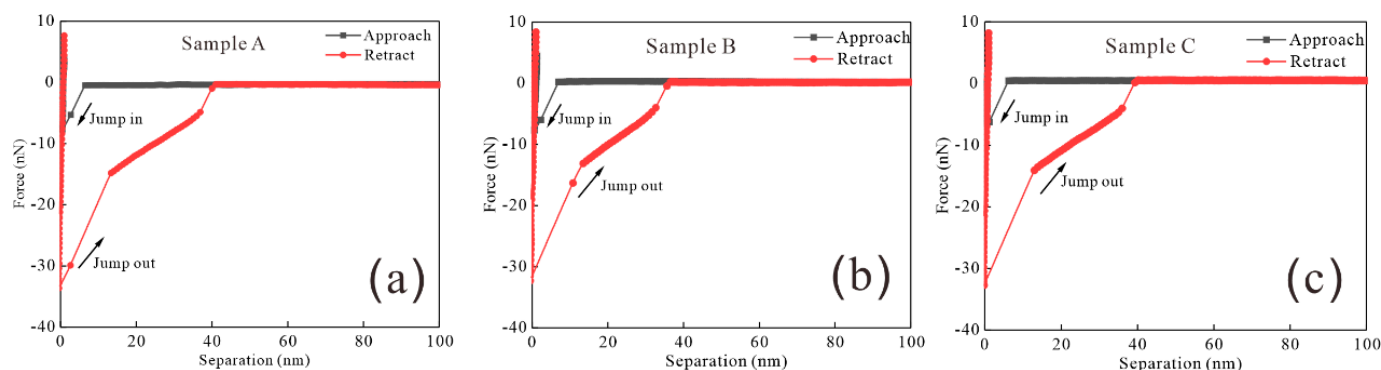


Figure 5. The adhesion force curves of shale oil on mica surface detect by AFM: (a) Sample A; (b) Sample B; (c) Sample C.

There are “jump-in” and “jump-out” phenomena in the force curves of the mica samples (Figure 5). Mica Sample A with the largest roughness is the first sample to show the “jump-in” phenomenon during the approach, and also the first to show the “jump-out” phenomenon. As the roughness decreases, the distance between the probe tip and mica surface gradually decreases when the “jump-in” phenomenon occurs. On the contrary, the

distance between the probe tip and sample surface increases with the increasing surface roughness when the “jump-out” phenomenon occurs. The position where the “jump out” behavior begins to occur can be approximately considered as the point with the maximum adhesion force. The maximum adhesion force of samples A, B and C are 30 nN, 17 nN, and 14 nN, respectively. Thus, the adhesion forces between shale oil and mica increase with the increase in the surface roughness.

4. Discussion

4.1. Relationship between Surface Roughness and Wettability

The wettability of sedimentary rocks is one of the hotspots during oil recovery. Many investigators measured the contact angle of tight sandstones, clay minerals, and shales, and found that mineral compositions affect the wettability of rocks [29,30]. In addition to minerals, the surface roughness and undulating morphology also bring uncertainty to the wettability. Our results show that the contact angle increases with the increase in the surface roughness (Figure 4).

One of the premises in Young’s equation is that the solid surface is smooth and the surface energy is homogeneous. However, the surface roughness will result in an unstable state of the droplet on a solid surface. This is mainly caused by the uncertainty of whether the fluid fully enters into the space between the rising and falling peaks or not. Consequently, there may be residual gas molecules between the rising and falling peaks, resulting in a solid–liquid–gas three-phase state. Based on this conjecture, Wenzel [31] assumed that when liquid droplets are located on a rough solid substrate, they can enter into and fill grooves in the rough structure, resulting in “wet contact” (Figure 6). In equilibrium state, the relation between the actual contact angle θ_w of a rough surface and the intrinsic contact angle θ in Young’s equation can be expressed as [31]:

$$\cos \theta_w = \frac{r(\gamma_{sg} - \gamma_{sl})}{\gamma_{gl}} = r \cos \theta \quad (11)$$

where r is surface roughness factor, and numerically equal to the ratio of the actual contact area of rough surface (A_r) to the geometrically contact area (A) between the droplet and smooth surface. It is difficult to obtain the actual contact area (A_r). Here, we proposed a method to calculate the A_r , which can be expressed as:

$$\frac{\cos \theta_{w1}}{\cos \theta_{w2}} = \frac{r_1 \cos \theta_1}{r_2 \cos \theta_2} \approx \frac{r_1}{r_2} \quad (12)$$

where subscripts 1 and 2 refer to Sample 1 and Sample 2, respectively. Sample 1 and Sample 2 are the same kinds of material, and only differ in surface roughness. In Equation (12), $\cos \theta$ represents the contact angle in the ideal state. Therefore, under ideal conditions, oil droplets have the same contact angles as the absolutely smooth surfaces of Sample 1 and Sample 2. Based on this judgment, $\cos \theta_1$ and $\cos \theta_2$ should be equal. Bittoun and Marmur conducted a wettability analysis for the cylindrical single convex structure model [28]. In this cylindrical model (Figure 7a), the base material is a square with lengths of the unit length (always set as 1). The surface roughness factor r_1 that consists of cylindrical pillars is the area of the cylinder that is exposed to the liquid (upper and lateral surface areas $\pi R^2 + 2\pi R h_1$, and the rest of the unit cell that is not covered by the cylinder $1 - \pi R^2$), divided by the projected area, which is the area of the unit cell. The surface roughness factor r_1 is then given by:

$$r_1 = 1 + 2\pi R h_1 \quad (13)$$

According to the definition of average roughness (Equation (1)), the average roughness for the cylindrical model in Figure 7a is h_1 ($R_{a1} = h_1$). When the height of the cylindrical

model changes, other parameters change as well (Figure 7b). The surface roughness factor r_2 is then given by:

$$r_2 = 1 + 2\pi R h_2 \quad (14)$$

Under the ideal condition, the average roughness is the height of the cylindrical pillars according to the definition of average roughness ($R_a = h$). If the h_1 and h_2 are much higher than the unit length, we can obtain:

$$\frac{r_1}{r_2} = \frac{1 + 2\pi R h_1}{1 + 2\pi R h_2} \approx \frac{h_1}{h_2} = \frac{R_{a1}}{R_{a2}} \quad (15)$$

From Equation (15), we can see that the ratio of r_1 to r_2 is approximately numerically equal to the average roughness R_{a1} to R_{a2} . Following this, we substitute the contact angle and average roughness measured in this experiment into Equation (15) for testing. The results show that the error of the ratio of the sample A to sample B is 10.4%, the error of the ratio of the sample A to sample C is 6.1% and the error of the ratio of the sample B to sample C is 3.5%. This fits well with the Wenzel model. In this way, we transformed the surface roughness factor r which is difficult to measure into the average roughness (R_a) which is easier to obtain.

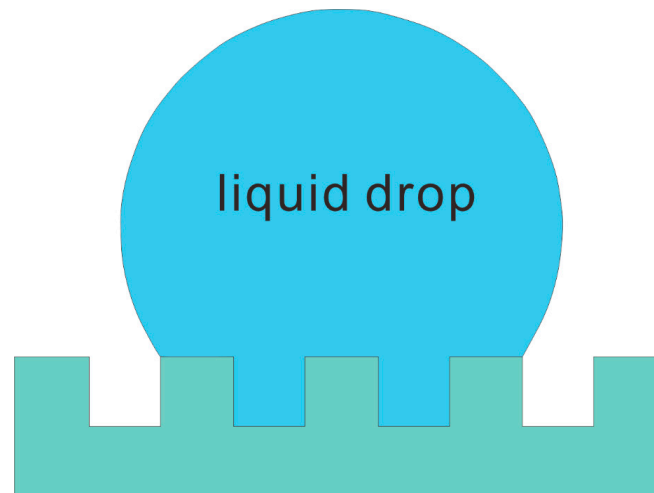


Figure 6. The wettability model describing the liquid droplets filling the grooves of the rough solid substrate.

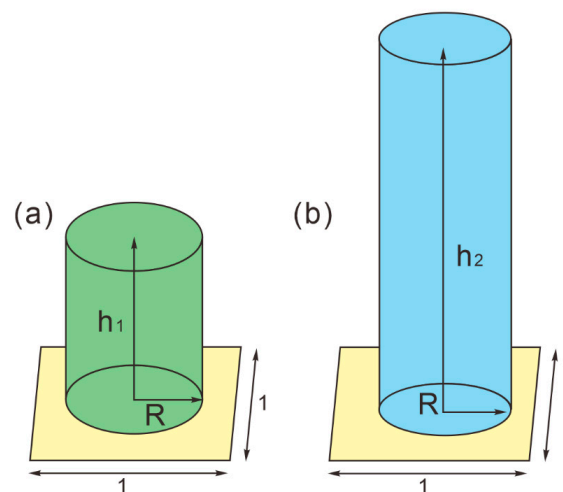


Figure 7. Unit cells of different height cylinder solid surface topographies: (a) Height of h_1 ; (b) Height of h_2 .

4.2. Effect of Surface Roughness on Adhesion Force

From the force curves of the micas samples (Figure 5), it can be seen that roughness affects the adhesion force between shale oil and micas. As the mineral surface roughness increases, the adhesion between minerals and shale oil droplets increases (Figure 5). The increase in roughness leads to an enlarged contacted area between the oil droplets and the mineral surface. If the adhesion force is mainly associated with the van der Waals force, the increase in the contacted area will increase the number of contacted molecules between the oil droplets and the mica surface, which leads to a higher adhesion force.

Since the fluid–rock interaction varies with the surface roughness, geological factors may change the roughness of rocks and thus the adhesion of oil in the reservoirs. For example, if rock matrixes are dissolved by the generated acid during the thermal maturity of organic matter in shales, the rock surfaces become unsmooth [32,33], and oil droplets will stick more tightly to the rock surface. Of course, this kind of adhesion intensity of crude oil in the pores is related to the action time. Recently, some researchers used the SFA to investigate the effect of the adsorption time of crude oil on the mica surface during the stripping behavior, and found that the longer the crude oil is adsorbed on the mineral surface, the stronger the adhesion [34]. It should be noted that in addition to adhesions, there are shear stresses when oil flows in porous media. Some researchers used rheology to study the effect of different levels of roughness on oil flow in porous media. It was found that the rough surface penetrated the slip layer and created a nonslip region, whereas the smooth plate showed a significantly higher slip at higher concentrations of particles [34,35]. In the future, we will conduct these investigations to verify the AFM detected results.

4.3. Jump-In and Jump-Out Behaviors

“Jump-in” and “jump-out” behaviors are commonly observed in the surfaces of both hard and soft materials during force measurements using AFM. Many researchers proposed different views on these particular behaviors [35,36]. It can be seen from the force curves that the “jump-in” behavior occurs at a very close distance between the oil-coated tip and the substrate sample (Figure 5). At this distance, the oil-coated probe tip does not yet contact the substrate surface, thus the “jump-in” behavior is probably caused by the hydrophilic interaction between the oxygen-containing functional group of crude oil and mica [36]. The “jump-in” behavior is followed by a slight increase in the repulsive force. After that, a large transformation occurs in the mica surface when the oil-coated probe tip contacts the mica surface and is further pressed (Figure 5). The “jump-out” behaviour is similar to “jump-in”, and occurs when the probe tip is moving away from the sample surface. Some studies also found that, considering the mechanical characteristics, both of these two deformations occur at positions where the force gradient is equal to or slightly higher than the stiffness of micro-cantilever beam of AFM [36].

4.4. Implications to the Shale Oil Occurrence

Shale oil mainly occurs as a free state and adsorption state in the pore systems of reservoirs [37,38]. Free shale oil is movable and mainly stored in large pores and fractures, including lamina, interbedded fractures, and dissolution-related pores [39,40]. Adsorbed shale oil is stored in organic matter-hosted pores and intercrystalline pores of clay minerals [39]. Taking micas as a representative clay mineral, we measured the adhesion between crude oil and mica. The strong adhesion is related to the asphaltenes and non-hydrocarbon components in crude oil, which are easily adsorbed on mineral surfaces in the form of ionic or hydrogen bonds [39]. The “wet contact” model proposed in the Wenzel model describes the filling behavior of hydrocarbons in the deep valleys of the rough surface, and forms microscopic spaces to store oil droplets [31]. The crude oil on the mica surface has a layered structure, where the polar groups such as hydroxyl (-OH) is toward mica and non-polar groups such as methyl (-CH₃) is toward the outside [40]. Crude oil molecules are adsorbed layer by layer on the surface of mica. Among them, the crude oil molecules in the first layer cannot move freely like the molecules in the outer layers. The thickness of the adsorbed

layer may be up to several nanometers according to the molecular simulation [41,42]. In addition, when crude oil molecules are adsorbed in the pores of organic matter, they show much stronger adhesion and thicker adsorption layers than in inorganic minerals, resulting in a more difficult movement of hydrocarbons in the organic matter-hosted pores. The high adhesion force between the crude oil and rock surface indicates that a considerable amount of energy is needed to separate hydrocarbon molecules from the pore space of shales.

The microscopic study about the wettability and adhesion of minerals provides new insights to shale oil recovery. Chemical additives with small molecules can be added and penetrate into crude oil and rough rock surfaces. Some studies have shown that the wettability of rocks can be reversed by adding nanomaterials [43]. As shown in Figure 8, nanoparticles in the three-phase contact region exert structural disjoining pressure, which drives the spreading of nanofluids by forming a continuous wedge film between the crude oil and solid surface [44,45]. The wetting and spreading of nanoparticles on solid substrates can be divided into two stages. In the first stage, nanoparticles rapidly spread on a solid surface by gravity and capillary forces. In the second stage, a wedge-film appears at the front of the solid–liquid interface. The nanoparticles are arranged in an orderly manner in the wedge-film, which leads to additional structural disjoining pressure. This structural disjoining pressure includes van der Waals forces, double electric repulsion, hydrogen bonding, etc. Among these forces, the double electric layer force is worth noting as the mica’s surface is charged when it contacts the aqueous solution or other polar solutions. There are polar components in the crude oil and even a certain amount of water in the produced fluid from the reservoir, which causes the surface of the oil and mica to be charged, and creates double electric layer force. Compared with the van der Waals force, the double electric layer force is a distant force, which shows greater repulsion between two surfaces. According to this characteristic, the double electric layer force may be the key for the crude oil droplets to detach from the rock surface. This provides the theoretical basis for the water injection with variable salinity in many oilfields [46]. In the future, we will focus on quantitatively characterizing the adsorption layer of shale oil on different minerals, and analyze the occurrence and movability of shale oil.

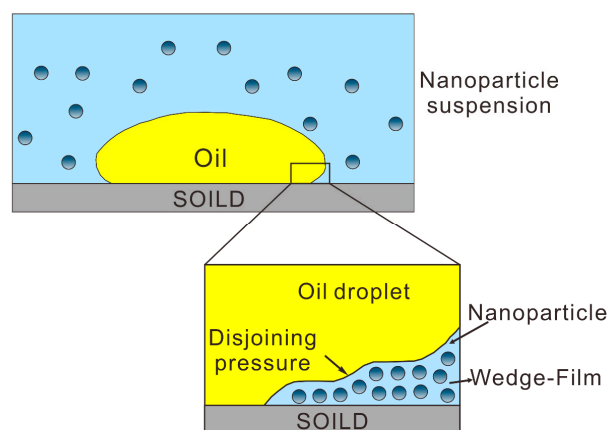


Figure 8. Nanoparticle structuring in the wedge film resulting in a structural disjoining pressure gradient at the wedge (modified from [45]).

5. Conclusions

This study investigated the adhesion of crude oil on mica using atomic force microscopy. Both 2D and 3D morphologies of micas were described and the average roughness of the mica surface was calculated. Taking the crude oil produced from a shale oil well drilling through the Yanchang Formation of the Ordos Basin as the experimental fluid, the contact angles of crude oil on micas were measured. The adhesion force curves between crude oil and mica were finely measured using crude oil-coated probe tips. The following main conclusions were drawn:

- (1) The surface of mica is not absolutely smooth. The maximum height drop of the mica surface is up to 4 nm, and the average roughness of micas is below 1 nm.
- (2) The contact angle between crude oil droplets and mica ranges from 128.7° to 145.8°, and increases with increasing surface roughness. The crude oil droplets fill the grooves in the rough surface of the mica, and thus form ‘wet contact’. The ‘wet contact’ provides microscopic storage spaces for crude oil droplets on rocks.
- (3) According to adhesion force measurements between oil droplets and mica surfaces, it was found that the adhesion force increases with increasing roughness. The maximum adhesion force between shale oil droplets and micas is between 14 and 30 nN. The maximum attraction force is reached at a distance of about 5–10 nm. The attraction force vanishes when the distance is greater than 40 nm.
- (4) The “jump-in” and “jump-out” behaviors during the force measurements are probably caused by the hydrophilic interaction between the oxygen-containing functional group of crude oil and mica. The hydrophilic interaction affects the layered accumulation of crude oil on the mica surface. The recovery of crude oil requires a decrease in the adhesion force to separate hydrocarbon molecules from the pore space of shales.

Author Contributions: Conceptualization, H.Z.; Data curation, T.B.; Funding acquisition, F.Y.; Investigation, T.B., F.Y. and H.W.; Methodology, H.Z.; Writing—original draft, T.B.; Writing—review & editing, F.Y. All authors have read and agreed to the published version of the manuscript.

Funding: This research was funded by the National Natural Science Foundation of China (Grant No. 42172180), the Science and Technology Research Project for the China National Petroleum Corporation (No. 2021DJ1802), the Key Laboratory of Petroleum Resources Research, Gansu Province (SZDKFJJ20211004), and the Open Research Fund of Teaching Laboratory, Wuhan, China University of Geosciences (No. SKJ2021016).

Institutional Review Board Statement: Not applicable.

Informed Consent Statement: Not applicable.

Data Availability Statement: The data presented in this study is available on request from the corresponding author.

Conflicts of Interest: The authors declare no conflict of interest.

Nomenclature

A_{123}	Hamaker constant for the tip and the sample surface (J)
D	separation distance between the tip and the sample surface (m)
F_{edl}	electrical double layer forces force (N)
F_{vdW}	van der Waals forces (N)
k	Boltzmann’s constant (1.381×10^{-23} J/K)
R	tip radius (m)
R_a	average roughness (nm)
R_q	root mean square roughness (nm)
T	temperature (K)
N_x	the number of scanning points along the X-axis of the image, respectively
N_y	the number of scanning points along the Y-axis of the image, respectively
Z_{mean}	the average height of all scanning points in the AFM image (nm)
α	geometric angle for the spherical cap at the tip end
ϵ	relative permittivity of medium
ϵ_0	permittivity of vacuum (8.854×10^{-12} F/m)
κ^{-1}	Debye length
ψ	surface potential (V)
θ	numerical value contact angle
θ_w	actual contact angle
h	height of cylinder solid surface topographies

References

1. Teklu, T.W.; Alameri, W.; Graves, R.M.; Kazemi, H.; Alsumaiti, A.M. Low-salinity water-alternating-CO₂ EOR. *J. Pet. Sci. Eng.* **2016**, *142*, 101–118. [[CrossRef](#)]
2. Manshad, A.K.; Rezaei, M.; Moradi, S.; Nowrouzi, I.; Mohammadi, A.H. Wettability alteration and interfacial tension (IFT) reduction in enhanced oil recovery (EOR) process by ionic liquid flooding. *J. Mol. Liq.* **2017**, *248*, 153–162. [[CrossRef](#)]
3. Makkonen, L. Young's equation revisited. *J. Phys. Condens. Matter* **2016**, *28*, 135001. [[CrossRef](#)] [[PubMed](#)]
4. Ma, B.Y.; Hu, Q.H.; Yang, S.Y.; Qiao, H.; Pu, X.; Han, W. An improved liquid-liquid extraction technique to determine shale wettability. *Mar. Pet. Geol.* **2022**, *138*, 105538. [[CrossRef](#)]
5. Xu, S.; Yassin, M.R.; Dehghanpour, H.; Kolbeck, C. The effects of kerogen maturity on pore structure and wettability of organic-rich calcareous shales. *J. Mol. Liq.* **2022**, *362*, 119577. [[CrossRef](#)]
6. Alnoush, W.; Sayed, A.; Solling, T.I.; Alyafei, N. Impact of calcite surface roughness in wettability assessment: Interferometry and atomic force microscopy analysis. *J. Pet. Sci. Eng.* **2021**, *203*, 108679. [[CrossRef](#)]
7. Wang, Y.; Xia, Y.; Feng, Z.; Shao, H.; Qiu, J.; Ma, S.; Zhang, J.; Jiang, H.; Li, J.; Gao, B.; et al. Microscale evaluation of tight oil mobility: Insights from pore network simulation. *Energies* **2021**, *14*, 4580. [[CrossRef](#)]
8. Gao, H.; Zhou, X.; Wen, Z.; Guo, W.; Tian, W.; Li, S.; Fan, Y.; Luo, Y. Classification and evaluation of shale oil reservoirs of the Chang 71-2 Sub-Member in the Longdong area. *Energies* **2022**, *15*, 5364. [[CrossRef](#)]
9. Zhao, F.; Dong, Z.; Wang, C.; Zhang, W.; Yu, R. Pore connectivity characteristics and controlling factors for black shales in the Wufeng-Longmaxi Formation, Southeastern Sichuan Basin, China. *Energies* **2022**, *15*, 2909. [[CrossRef](#)]
10. Abudu, A.; Goual, L. Adsorption of crude oil on surfaces using quartz crystal microbalance with dissipation (QCM-D) under flow conditions. *Energy Fuels* **2009**, *23*, 1237–1248. [[CrossRef](#)]
11. Huang, J.; Stoyanov, S.R.; Zeng, H. A comparison study on adsorption and interaction behaviors of diluted bitumen and conventional crude oil on model mineral surface. *Fuel* **2019**, *253*, 383–391. [[CrossRef](#)]
12. Liu, J.; Wang, J.; Huang, J.; Cui, X.; Tan, X.; Liu, Q.; Zeng, H. Heterogeneous distribution of adsorbed bitumen on fine solids from solvent-based extraction of oil sands probed by AFM. *Energy Fuels* **2017**, *31*, 8833–8842. [[CrossRef](#)]
13. Liu, X.; Yan, W.; Stenby, E.H.; Thormann, E. Release of crude oil from silica and calcium carbonate surfaces: On the alternation of surface and molecular forces by high- and low-salinity aqueous salt solutions. *Energy Fuels* **2016**, *30*, 3986–3993. [[CrossRef](#)]
14. Zhu, C.; Li, G.; Xing, Y.; Gui, X. Adhesion forces for water/oil droplet and bubble on coking coal surfaces with different roughness. *Int. J. Min. Sci. Technol.* **2021**, *31*, 681–687. [[CrossRef](#)]
15. Natarajan, A.; Kuznicki, N.; Harbottle, D.; Masliyah, J.; Zeng, H.B.; Xu, Z.H. Understanding mechanisms of asphaltene adsorption from organic solvent on mica. *Langmuir* **2014**, *30*, 9370–9377. [[CrossRef](#)] [[PubMed](#)]
16. Stewart, M.P.; Hodel, A.W.; Spielhofer, A.; Cattin, C.J.; Muller, D.J.; Helenius, J. Wedged AFM-cantilevers for parallel plate cell mechanics. *Methods* **2013**, *60*, 186–194. [[CrossRef](#)]
17. Zhao, S.; Li, Y.; Wang, Y.; Ma, Z.; Huang, X. Quantitative study on coal and shale pore structure and surface roughness based on atomic force microscopy and image processing. *Fuel* **2019**, *244*, 78–90. [[CrossRef](#)]
18. Smith, J.R.; Larson, C.; Campbell, S.A. Recent applications of SEM and AFM for assessing topography of metal and related coatings—a review. *Trans. IMF* **2011**, *89*, 18–27. [[CrossRef](#)]
19. Li, C.; Ostadhassan, M.; Guo, S.; Gentzis, T.; Kong, L. Application of peak force tapping mode of atomic force microscope to characterize nanomechanical properties of organic matter of the Bakken Shale. *Fuel* **2018**, *233*, 894–910. [[CrossRef](#)]
20. Dickinson, L.R.; Suijkerbuijk, B.M.J.M.; Berg, S.; Marcelis, F.H.M.; Schniepp, H.C. Atomic Force Spectroscopy Using Colloidal Tips Functionalized with Dried Crude Oil: A Versatile Tool to Investigate Oil-Mineral Interactions. *Energy Fuels* **2016**, *30*, 9193–9202. [[CrossRef](#)]
21. Okabe, Y.; Akiba, U.; Fujihira, M. Chemical force microscopy of -CH₃ and -COOH terminal groups in mixed self-assembled monolayers by pulsed-force-mode atomic force microscopy. *Appl. Surf. Sci.* **2000**, *157*, 398–404. [[CrossRef](#)]
22. Okabe, Y.; Furugori, M.; Tani, Y.; Akiba, U.; Fujihira, M. Chemical force microscopy of microcontact-printed self-assembled monolayers by pulsed-force-mode atomic force microscopy. *Ultramicroscopy* **2000**, *82*, 203–212. [[CrossRef](#)]
23. Chan, D.Y.C.; Dagastine, R.R.; White, L.R. Forces between a rigid probe particle and a liquid interface. I. The repulsive case. *J. Colloid Interface Sci.* **2001**, *236*, 141–154. [[CrossRef](#)] [[PubMed](#)]
24. Liu, J.; Xu, Z.; Masliyah, J. Studies on bitumen-silica interaction in aqueous solutions by atomic force microscopy. *Langmuir* **2003**, *19*, 3911–3920. [[CrossRef](#)]
25. Shang, X.Y.; Zhao, K.; Qian, W.X.; Zhu, Q.Y.; Zhou, G.Q. On the calculation of van der Waals force between clay particles. *Minerals* **2020**, *10*, 993. [[CrossRef](#)]
26. Barattin, R.; Voyer, N. Chemical modifications of AFM tips for the study of molecular recognition events. *Chem. Commun.* **2008**, *13*, 1513–1532. [[CrossRef](#)]
27. Drelich, J.; Long, J.; Yeung, A. Determining surface potential of the bitumen-water interface at nanoscale resolution using atomic force microscopy. *Can. J. Chem. Eng.* **2007**, *85*, 625–634. [[CrossRef](#)]
28. Hutter, J.L.; Bechhoefer, J. Calibration of atomic-force microscope tips. *Rev. Sci. Instrum.* **1993**, *64*, 1868–1873. [[CrossRef](#)]
29. Wang, L.; Fu, Y.; Li, J.; Sima, L.; Wu, Q.; Jin, W.; Wang, T. Experimental study on the wettability of Longmaxi gas shale from Jiaoshiha gas field, Sichuan Basin, China. *J. Pet. Sci. Eng.* **2017**, *151*, 488–495. [[CrossRef](#)]

30. Yang, F.; Zheng, H.; Guo, Q.; Lyu, B.; Nie, S.; Wang, H. Modeling water imbibition and penetration in shales: New insights into the retention of fracturing fluids. *Energy Fuels* **2021**, *35*, 13776–13787. [[CrossRef](#)]
31. Wenzel, R.N. Resistance of solid surfaces to wetting by water. *Ind. Eng. Chem.* **1936**, *28*, 988–994. [[CrossRef](#)]
32. Bittoun, E.; Marmur, A. Optimizing Super-Hydrophobic Surfaces: Criteria for Comparison of Surface Topographies. *J. Adhes. Sci. Technol.* **2009**, *23*, 401–411. [[CrossRef](#)]
33. Liu, S.B.; Huang, S.J.; Shen, Z.M.; Lü, Z.X.; Song, R.C. Diagenetic fluid evolution and water-rock interaction model of carbonate cements in sandstone: An example from the reservoir sandstone of the Fourth Member of the Xujiahe Formation of the Xiaoquan-Fenggu area, Sichuan Province, China. *Sci. China Earth Sci.* **2014**, *57*, 1077–1092. [[CrossRef](#)]
34. Abbasi Moud, A.; Piette, J.; Danesh, M.; Georgiou, G.C.; Hatzikiriakos, S.G. Apparent slip in colloidal suspensions. *J. Rheol.* **2022**, *66*, 79–90. [[CrossRef](#)]
35. Piette, J.; Moud, A.A.; Poisson, J.; Derakhshandeh, B.; Hudson, Z.M.; Hatzikiriakos, S.G. Rheology of mature fine tailings. *Phy. Fluids* **2022**, *34*, 063104. [[CrossRef](#)]
36. Zhang, L.; Shi, C.; Lu, Q.; Liu, Q.; Zeng, H. Probing molecular interactions of asphaltenes in heptol using a surface forces apparatus: Implications on stability of water-in-oil emulsions. *Langmuir* **2016**, *32*, 4886–4895. [[CrossRef](#)] [[PubMed](#)]
37. Wang, M.; Ma, R.; Li, J.; Lu, S.; Li, C.; Guo, Z.; Li, Z. Occurrence mechanism of lacustrine shale oil in the Paleogene Shahejie Formation of Jiyang Depression, Bohai Bay Basin, China. *Pet. Explor. Dev.* **2019**, *46*, 833–846. [[CrossRef](#)]
38. Li, J.Q.; Lu, S.F.; Cai, J.C.; Zhang, P.F.; Xue, H.T.; Zhao, X.B. Adsorbed and free oil in lacustrine nanoporous shale: A theoretical model and a case study. *Energy Fuels* **2018**, *32*, 12247–12258. [[CrossRef](#)]
39. Guo, Q.; Pan, S.; Yang, F.; Yao, Y.; Zheng, H. Characterizing shale oil occurrence in the Yanchang Formation of the Ordos Basin, assisted by petrophysical and geochemical approaches. *Energy Fuels* **2022**, *36*, 370–381. [[CrossRef](#)]
40. Han, Y.; Mahlstedt, N.; Horsfield, B. The Barnett Shale: Compositional fractionation associated with intraformational petroleum migration, retention, and expulsion. *AAPG Bull.* **2015**, *99*, 2173–2202. [[CrossRef](#)]
41. Yang, Y.Y.; Liu, J.; Yao, J.; Kou, J.L.; Li, Z.; Wu, T.H.; Zhang, K.; Zhang, L.; Sun, H. Adsorption behaviors of shale oil in kerogen slit by molecular simulation. *Chem. Eng. J.* **2020**, *387*, 124054. [[CrossRef](#)]
42. Zhao, G.; Tan, Q.Y.; Xiang, L.; Cai, D.; Zeng, H.B.; Yi, H.; Ni, Z.H.; Chen, Y.F. Structure and properties of water film adsorbed on mica surfaces. *J. Chem. Phys.* **2015**, *143*, 104705. [[CrossRef](#)] [[PubMed](#)]
43. Wang, L.; Song, Y.; Zhang, B.; Wang, E. Adsorption behaviors of methanol, ethanol, n-butanol, n-hexanol and n-octanol on mica surface studied by atomic force microscopy. *Thin Solid Films* **2004**, *458*, 197–202. [[CrossRef](#)]
44. Al-Ansari, S.; Wang, S.; Barifcani, A.; Lebedev, M.; Iglauer, S. Effect of temperature and SiO₂ nanoparticle size on wettability alteration of oil-wet calcite. *Fuel* **2017**, *206*, 34–42. [[CrossRef](#)]
45. Kondiparty, K.; Nikolov, A.D.; Wasan, D.; Liu, K. Dynamic spreading of nano fluids on solids. Part I: Experimental. *Langmuir* **2012**, *28*, 14618–14623. [[CrossRef](#)]
46. Liu, K.L.; Kondiparty, K.; Nikolov, A.D.; Wasan, D. Dynamic spreading of nanofluids on solids part II: Modeling. *Langmuir* **2012**, *28*, 16274–16284. [[CrossRef](#)]